SLOW STRAIN RATE TENSILE TESTS ON HP-40 AUSTENITIC STAINLESS STEEL[1]

Simon Pérusin[2]
Raphaëlle Peraldi[2]
Jacques Lacaze[2]
Jader Ferreira Furtado Filho[3]
Eric Andrieu[2]

Abstract
HP-40 austenitic stainless steel alloyed with Nb is presently used as material for reformer tubes that are manufactured by centrifugation. The as-cast microstructure consists of a dendritic matrix delineated by a network of NbC and M_7C_3 carbide types. While this carbide network helps improving creep resistance during normal service, experiments performed during the present study showed it to be detrimental in case of slow strain rate tensile tests at higher temperature. This suggests that this material can hardly support non-uniform loadings such as those building up during temperature overshoots in service. This could possibly explain short term failures of tubes in reforming plants as repeatedly reported in the literature.
Key words: HP-40 stainless steel; Slow strain rate tensile tests; Chromium carbides; Niobium carbides; Cracks

[1] *Technical Contribution to the 61st International Congress of the ABM, January 24-27th 2006, Rio de Janeiro – RJ – Brazil.*
[2] *CIRIMAT UMR 5085, ENSIACET-INPT, 31077 Toulouse Cedex 4, France*
[3] *Member of ABM, AIR LIQUIDE CRCD, BP 126 - Les Loges-en-Josas, 78 350 Jouy-en-Josas Cedex, France*

INTRODUCTION

Centrifugally cast austenitic stainless steels such as HK-40 (25 Cr, 20 Ni, 0.4 C, in wt. % all along the text) and modified or microalloyed HP-40 stainless steel (25 Cr, 35 Ni, 0.4 C) are widely used as reformer tubes by the petrochemical industry in ammonia, methanol and syngas plants. In most of the cases, methane is used as feedstock and driven to react with steam in catalyst-packed tubes at high temperature to produce syngas, a gas mixture of CO and H_2. The tubes have inside diameters of 60 to 120 mm and are 10 to 14 m long. The process is endothermic so that the mixture of hydrocarbons and steam is subjected to a pressure in the range of 10 to 40 bars and it is heated above 850°C from outside the tubes using burners. It is now well accepted [1-3] that temperature overshoots can occur especially in the bottom part of the tubes due to the process design.

The better creep properties of HP-40 modified Nb alloy with respect to HK-40 alloy have allowed the internal volume of the tubes to be enlarged at constant tube wall thickness, leading to a production increase of 30 to 40 %. This replacement is based on the American Petroleum Institute (API) recommended practice 530 [3] using a nominal life of 100 000 h (11.4 years) in service conditions. As the principal degradation mechanism leading to failure in service is well recognised to be creep [4-11], Larson-Miller extrapolation has been used for this design calculation. However, tubes failures at much shorter times have been repeatedly reported [2, 3, 9] that could be possibly related to temperature overshoots. While the effect of temperature on the microstructure of HP-40 alloy has been investigated, the mechanical properties of this alloy are much less documented. The present study was thus aimed at investigating the response of the material during tensile tests carried out at slow strain rate. These conditions are not far from those experienced by the tubes during overheatings.

The as cast microstructure of the HP-40 modified Nb alloy consists of an austenite matrix with Nb rich MC type and $(Fe,Cr)_7C_3$ type carbides in the interdendritic regions. This eutectic-like carbide network appears to play an important role in preventing grain boundary sliding during creep [7] although many cracks have been observed at their interface with the matrix after service exposure [4]. During service, the $(Fe,Cr)_7C_3$ type carbides are rapidly transformed in $M_{23}C_6$ carbides [12]. A secondary precipitation also occurs in the matrix after aging at high temperature [5, 13-16] that acts to restrict the motion of dislocations and contributes to increase the creep resistance of the alloy. Numerous works [9, 13, 15] have been dedicated to the study of the coarsening of these secondary precipitates on the creep properties of the alloys but there are surprisingly few studies concerning the mechanical behaviour of the interfaces between the network of eutectic carbides and the dendrites even if creep cracking is always observed at these interfaces.

This paper reports preliminary results obtained on as-cast HP-40 alloys of two origins during tensile tests carried out at slow strain rate. Small samples were used in order to look for any effect on the mechanical properties of the location within the tube thickness. The effects of the atmosphere (synthetic air vs. reducing atmosphere) and of the strain rate were also checked. Finally, a test on used on plant material was performed in order to seek for comparison.

EXPERIMENTAL PROCEDURE

The materials investigated were taken out from four tubes made of HP-40 stainless steel, three as-cast tubes labeled A, B1 and B2, and one used-on-plant tube labeled AU. Tubes A and AU come from the same manufacturer but do not have the same dimensions. Tubes B1 and B2 were cast with the same nominal conditions, i.e. the same chemical composition and centrifugation conditions, and should thus be considered as identical. Tube AU had been in service for an unknown duration, it was located in the upper part of the reformer so that the material was subject to temperatures below 900°C and did not suffer much from the overshoots and cooling-downs. Table 1 gives the inner and outer diameters of the tubes where it is seen that they have all the same outer diameter but that tube A is much thicker than the three other ones. Figure 1 presents an optical macrograph of the cross-section of the tube B after etching with Behara's solution (48g NH_4F-HF, 800 ml H_2O, 400 ml HCl). The material exhibits columnar grains across the whole thickness (15 to 16 mm) of the tube. The thicker tube presented a columnar zone in the outer part of the section, but also a equiaxe zone (10 mm thick) in the inner part.

label	inner/outer diameters (mm)	Fe	Ni	Cr	Nb	Si	Mn
A	86/138	37.2	32.6	25.5	1.0	1.5	1.3
AU	106/136	36.9	32.6	25.9	1.0	1.3	1.3
B1	106/138	34.7	34.9	26.0	1.4	0.6	0.7
B2	106/138	34.8	35.1	26.3	1.1	0.6	0.7

Table 1. Label of the tubes investigated in this study, dimensions and average compositions (wt. %) estimated by EDX.

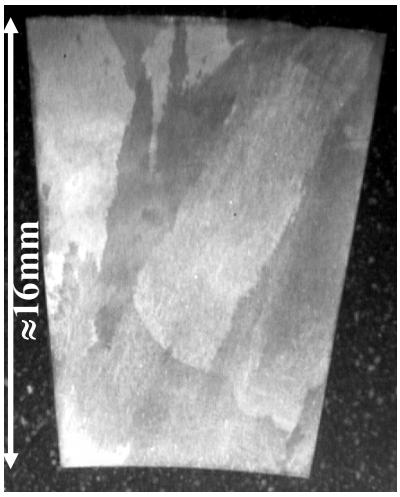

Figure 1. Optical macrograph through the tube thickness of as-cast B1 material.

Table 1 lists also the composition of the materials as evaluated on the section of the tubes by means of energy dispersive X-ray diffraction (EDX) in a scanning electron microscope (SEM). These compositions were obtained by averaging data recorded in raster mode on 10 to 15 fields through the tube thickness. It is seen that all materials present the same content in the main elements, Fe, Ni and Cr, about the same level of Nb, and that material B contains slightly lower amount of Si and Mn than material A. Neither the carbon content nor the amount of low level additions could be measured by EDX.

EDX analysis was also used in spot mode to identify the phases present in the materials. However, the composition ranges observed were too extended to allow of an unambiguous determination of the phases present, so that X-Ray diffraction (XRD) was also used. These latter analyses have been achieved on an area about 1.5 mm^2 in size located in the middle of the tubes section after polishing down to 2400 SiC paper. XRD patterns were recorded in the 2θ range 34° to 45° using Cu K_α radiation ($\lambda K_{\alpha 1}$=1.541 Å).

Specimens for slow strain rate tensile tests were machined with their axis parallel to the tube axis as illustrated in Figure 2-a. At first, samples with a gage section of 2x1 mm^2 were used which are represented in Figure 2-b. In a second step, the sample section was increased up to 4x2 mm^2 with all other dimensions unchanged. Before testing, the samples were mirror polished down to ¼ µm diamond paste and the edges of the gage length were ground using a 320 grade SiC paper to remove any defects induced by machining. After polishing, the dimensions of the gage were carefully measured using an optical microscope.

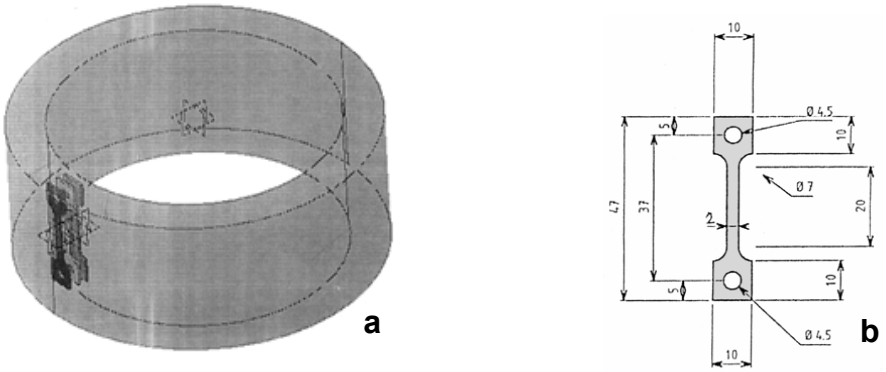

Figure 2. a) Schematic showing the sampling of the specimens in the tube thickness; b) dimensions of the 1 mm thick samples.

All tensile tests were performed at 1000 °C using a MTS electromechanical machine, with a load cell of 5000 N, which has been equipped with a four lamps furnace. During the heating up to 1000 °C (carried out at 50 °C.min^{-1}), the sample was maintained under slight tension to prevent from buckling due to thermal dilatation of the different parts of the machine. A 15 min dwell time was respected at 1000 °C before starting the mechanical test to allow for temperature homogenization of the sample. Two thermocouples welded on the top and bottom heads of the sample showed a maximum temperature difference of 10 °C along the 20 mm gage length. Unless otherwise specified, the tensile tests were performed in synthetic dry air (80 % N_2, 20 % O_2) at an initial strain rate of 10^{-5} s^{-1}. A laser extensometer was used to measure the relative displacement of two flags welded on the extremities of the gage length of the specimen, from which was evaluated the strain.

RESULTS

Microstructure Characterization

All as-cast materials showed a similar microstructure consisting in an austenitic matrix delineated by a network of interdendritic carbides typical of this kind of material [3, 9, 13-15, 17-21]. This is illustrated in Figure 3-a which is a SEM micrograph taken with a quadrature backscattering detector (QBSD) and in which carbides appearing in white contrast are rich in Nb and those dark grey are rich in Cr. These carbides have been identified using X-ray diffraction as MC and M_7C_3 as shows Figure 4-a. After aging in service in the upper part of the reformer, the microstructure of the material appears quite similar but the presence of so-called secondary precipitates within the dendrites as illustrated in Figure 3-b. As expected from the literature and illustrated in Figure 4-b, the nature of the interdendritic Cr-rich carbides has changed from M_7C_3 to $M_{23}C_6$. Some precipitates rich in Nb, Ni and Si,

and containing C, have also been detected by EDX in the interdendritic areas of the AU material. They should be precipitates of G phase ($Nb_6Ni_{16}Si_7$) or of the so-called silicon "version" of the η carbide [14].

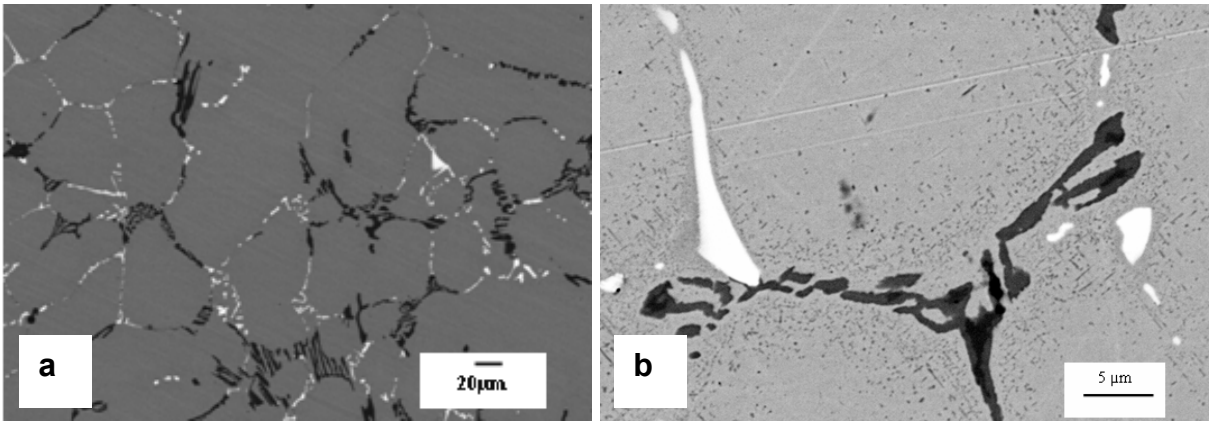

Figure 3. Microstructures of as-cast A material (a) and of used-on-plant AU material (b). Images obtained using backscattered electrons mode in SEM.

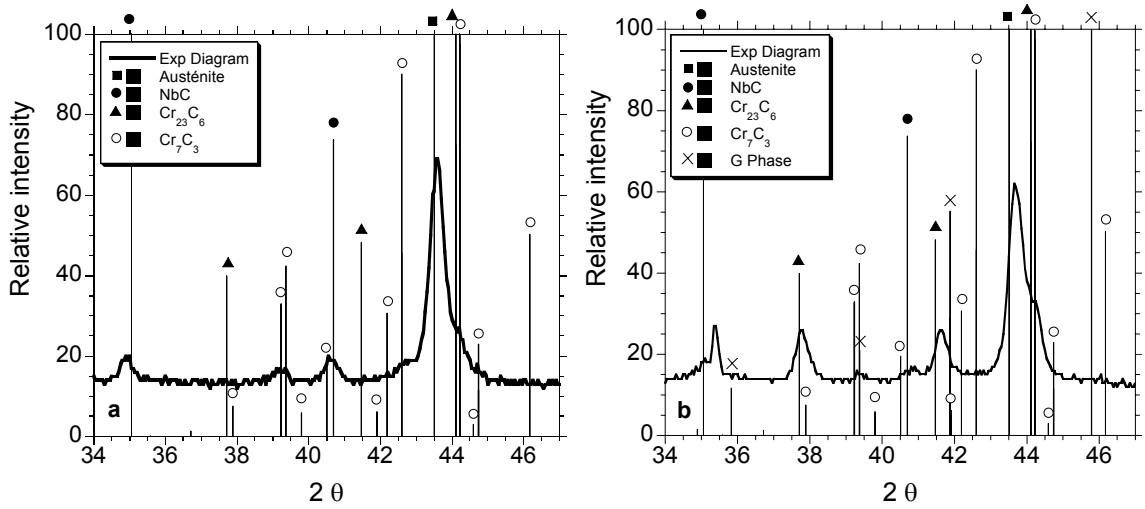

Figure 4. Experimental X-ray diagrams of as cast material A material (a) and of used-on-plant AU material (b). X-ray lines of the various phases expected to appear have been superimposed on the diagram.

Mechanical Testing

Four samples 1 mm thick (gage section 2x1 mm^2) were machined at regular interval from the section of tube B2, sample 1 being close to the outer surface and sample 4 close to the inner one. Figure 5 presents the true stress-true strain curves obtained, which all show a very peculiar behaviour, with the stress increasing up to a maximum of about 90 to 100 MPa for a strain of 0.5 %, then decreasing sharply as the strain increases further. The material thus appears to be strongly damaged as soon as the stress has reached a critical level. The present results may be in line with previous discussion on the behaviour of HK-40 alloy under tensile testing [4]. They also show that there is no significant effect of the position in the tube thickness on the maximum tensile stress that the material can sustain.

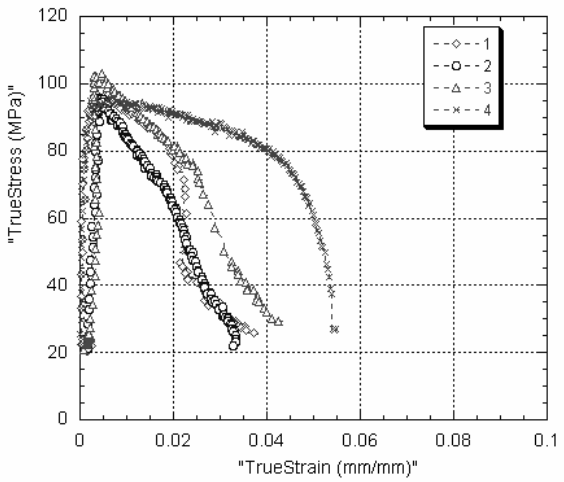

Figure 5. True stress-true strain curves of the as-cast B2 material (sample thickness 1 mm; temperature 1000 °C; strain rate $\dot{\varepsilon}=10^{-5}s^{-1}$; synthetic air). Samples 1 to 4 were taken from the outer to the inner surfaces of the tube.

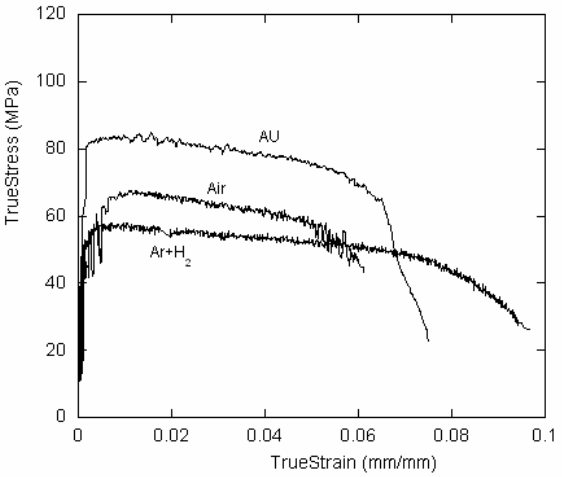

Figure 6. True stress-true strain curves of the as-cast A material under either synthetic air and $Ar+H_2$, and of AU material under synthetic air (sample thickness: 1 mm, temperature: 1000 °C and strain rate $\dot{\varepsilon}=10^{-5}s^{-1}$ in all cases).

It has been verified that this peculiar behaviour could not be related to the atmosphere used to perform the test. This check was achieved by comparing the mechanical response of two samples taken out from tube A in the middle of the section, that were tested respectively in synthetic air and under reducing conditions (Ar+5 % H_2). The curves obtained are presented in Figure 6 and show little change from one to the other: the yield stress is slightly lower while the elongation at rupture is slightly higher for the sample tested in reducing atmosphere. SEM observation revealed the presence of numerous cracks in the gage length of both samples (see Figure 7-a), showing that crack nucleation and propagation is not a consequence of an oxidation process.

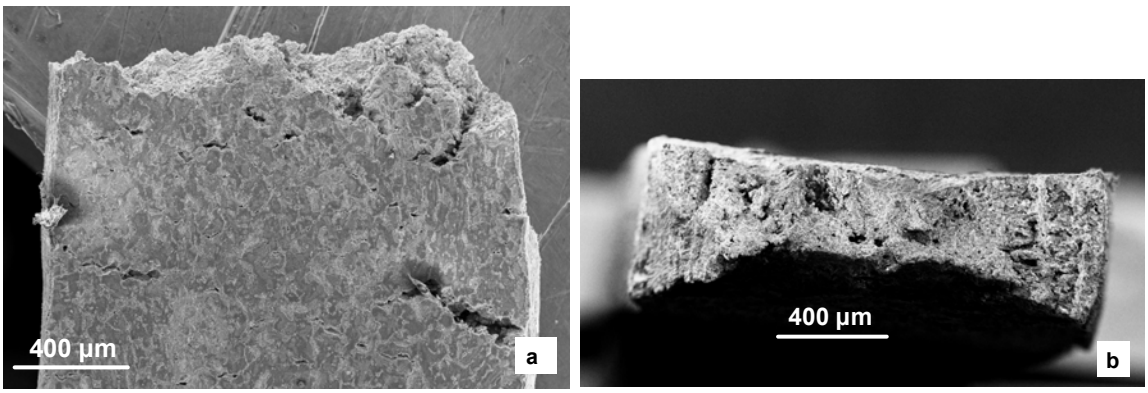

Figure 7. Fracture surface (a) and view of the gage surface (b) of the sample of A material. A primary trunk with dendrite arms is clearly seen in the right part of the fractured surface.

In Figure 6 has been also plotted the stress-strain curve recorded on a 1 mm thick sample taken out from the middle of the section of tube AU. It is seen that the curve presents about the same shape than for the two as-cast A samples, although the yield strength is significantly higher. This result could partly be due to the beneficial effect of the secondary precipitation observed in this sample (Figure 3-b),

though it has been reported that intradendritic precipitation starts at very short times during holding of the material at high temperature [12], and is thus expected to have appeared in the as-cast specimens during testing. As the dendritic structure of the AU material is slightly finer than the one of the A material, because of the respective thicknesses of the tubes, one may suggest that the level of the yield stress is also correlated to the topological properties of the internested dendritic and eutectic networks. This should be investigated further by comparing quantitatively the microstructure of A, AU and B2 materials.

This latter hypothesis is illustrated by the fact that, in many cases as in the right part of Figure 7-b, primary dendrite arms were easily visible on the fracture sections. This indicates that cracks have followed the primary eutectic carbides/matrix interfaces, in agreement with previous observations that the main feature of the damage in these types of materials is formed by cavities nucleating and growing at these interfaces. Then, the sharp decrease of the stress observed on the stress-strain curves could be tentatively related to crack propagation along the interface between the dendrites and the eutectic network. It is worth noting that the characteristic size of the dendrites, as given by the average size of their secondary arms, is quite large at about 40 to 50 µm (Figure 3-a) when compared to the 1 mm thickness of the test samples. It may thus be inferred that the stress-strain curves should depend on the thickness of the gage of the test sample.

Accordingly, samples with 4x2 mm^2 gage section were machined out from tube B1 in the middle of the section. Two of these samples were tested at 10^{-5} s^{-1} as before, giving quite reproducible stress-strain curves shown in Figure 8. It is noteworthy that the curves present a plateau rather than the sharp decrease seen in Figure 5 in case of alloy B2. Considering that B1 and B2 materials are identical as mentioned above, it is seen that the change of the gage section leads to an important increase of the facture strain but also to a significant decrease of the maximum stress. As in the case of the thin samples, many cracks localised in the interdendritic spaces were also well visible along the gage length of the thick samples (Figure 9). Most of these cracks have been observed near the final rupture and on the edges of the samples but some were located in the middle of the specimen far from the final fracture zone.

It may be suggested that the behaviour of the 2x1 mm^2 gage section samples of tube B2 (Figure 5) and of the 4x2 mm^2 gage section samples of tube B1 (Figure 8) are respectively controlled by the network of eutectic carbides and by the austenite dendrites. This hypothesis should be further investigated through detailed examination of the ruptured samples. The apparent ductility measured on the true stress-true strain curves would be in fact related to the propagation of cracks at the primary eutectic carbides/dendrites interfaces. The thicker the section of the sample, the higher the apparent ductility.

In the product information given by the manufacturers, tensile tests performed at a strain rate of 10^{-3} s^{-1} on large specimens give elongation to rupture values of about 40 % at 1000 °C [22, 23]. This value is two times higher than the value obtained at 10^{-5} s^{-1} on 2 mm thick samples in this study. Then, the influence of the strain rate on the mechanical properties of the as cast material has been evaluated by carrying out a test at 10^{-3} s^{-1} on a 2 mm thick sample. The stress-strain curve has been reported in Figure 8 to be compared with the curves at 10^{-5} s^{-1}. The Figure shows that the material has classical elasto-viscoplastic behaviour with positive strain rate sensitivity, the yield strength increasing with the strain rate. However, it is seen that the fracture strain is unchanged. The strain rate sensitivity exponent m defined as $m = \partial \ln \sigma / \partial \ln \dot{\varepsilon}$ can be calculated using the flow stresses obtained at 10^{-3} and 10^{-5}

s^{-1} (83 and 53 MPa respectively), giving m equal to 0.097. The inverse of m, 10 in that case, can be compared to the Norton coefficient n obtained in creep tests in previous results. In their work on HK-40 as cast alloy, Dunlop et al. [4] found a value of 9 for n which is well comparable to the sensitivity observed during the tensile tests carried out during the present study.

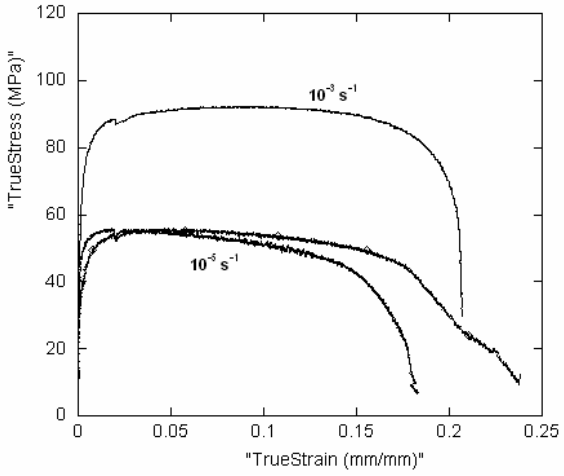

Figure 8. True stress-true strain curves of the as-cast B1 material (sample thickness: 2 mm; temperature: 1000 °C; synthetic air) strain rate at either 10^{-5} s^{-1} and 10^{-3} s^{-1}.

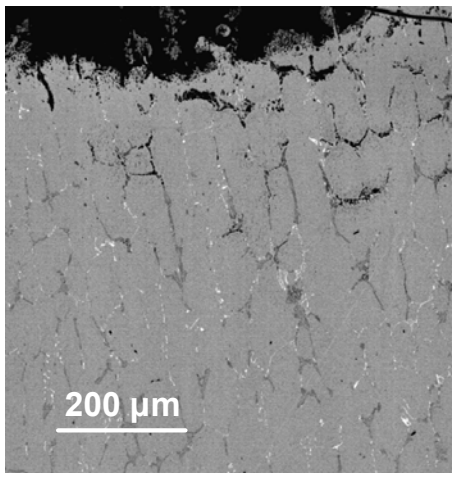

Figure 9. View of the polished surface of a 2 mm thick as-cast B1 specimen tested in tension at T=1000 °C, $\dot{\varepsilon} = 10^{-5}\,\mathrm{s}^{-1}$ under synthetic air.

DISCUSSION

Apart for thin samples of material B2, the stress-strain curves recorded in the present work showed a plateau at nearly constant stress. This experimental fact suggested comparing the present results to literature data on creep of HK-40 and HP-40 alloys [2, 6, 7, 9]. A Larson-Miller diagram was thus drawn as shown in Figure 10 from various previous works and using as Larson-Miller parameter $LMP=10^{-3}.T.[22.9+\log(t_r)]$, where T is the temperature in Kelvin and t_r the time to rupture in hours. Data on HK-40, HP-40 and HP-40 modified with niobium were originally reported by Kirchheiner and Woelpert [7] as creep resistance for 10^5 hours of service at temperature varying from 750 to 1100 °C. This information was converted to be plotted on the Larson-Miller diagram. Wu et al. [6] made experiments on HK-40 type alloy cast with three different centrifugation conditions. Their creep tests were carried out at 871 °C (60, 80 and 100 MPa) and 950 °C (30, 40 and 50 MPa) and they reported their results with a different LMP which was thus recalculated for plotting in Figure 10. Muralidharan et al. [9] compared the values of t_r for two HP-40 alloys, with 1 and 2 wt. % Nb, at 982 °C (27.6 MPa) and 1093 °C (13.8 and 6.9 MPa). Ray et al. [2] reported creep data obtained on used on plant material taken off the lower and upper parts of a tube. Their experiments were performed between 900 °C (maximum stress of 46.3 MPa) and 960 °C (33 MPa).

To plot the present results obtained under slow tensile testing, the stress was calculated as the arithmetic mean of the stress at the beginning of the plastic deformation and the one before the rapid decrease of the load before rupture. The rupture time t_r considered is the time effectively spent between these two characteristic points. The corresponding values have been reported with solid symbols on the diagram

in Figure 10. It is worth noting that the results obtained in slow strain rate tensile tests compare well with those of creep tests. This should indicate that the deformation mechanisms are not so different in creep and slow strain rate tensile tests when the stress is relatively high. This conclusion is sustained by the fact that the fracture surfaces observed during this work are similar to those reported in the literature for crept specimens, with numerous cracks developing at the interface between the dendrites and the eutectic network. At lower stress levels, it may be expected that other adaptation mechanisms are active during creep and that slow strain rate tensile tests could not be anymore compared with creep data. It is worth noticing in Figure 10 that a break in the slope is observed at high temperatures (LMP>37). It should thus be of great interest to perform creep test at low stress level and at lower temperature than those used up to now to investigate this part of the diagram.

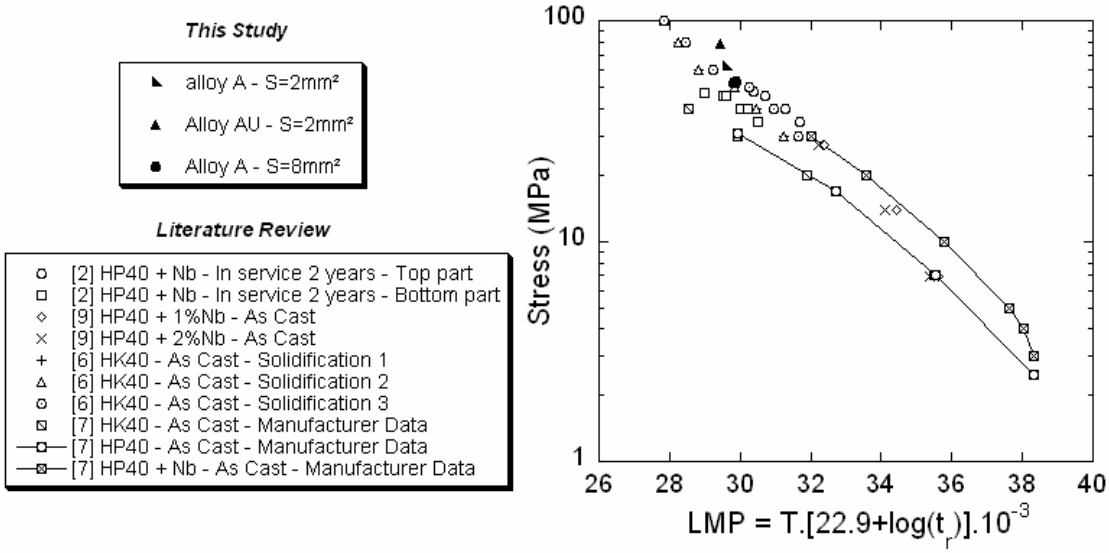

Figure 10. Larson-Miller curve built up with literature data of creep tests (open symbols and crosses) and results obtained in slow strain rate tensile tests in this study (solid symbols).

CONCLUSIONS

Experiments performed during the present study show that the network of MC and M_7C_3 (or $M_{23}C_6$) interdendritic carbides is detrimental in case of slow strain rate tensile tests carried out on HP-40 alloy at high temperature. Many cracks are indeed observed at the carbides/dendrites interfaces and their propagation is responsible for the fracture of the samples. As a consequence, the thinner the section of the sample, the shorter the propagation and the shorter the life duration. The measured fracture strain appears in fact as due to a cumulative damage of the sample. This behaviour of the material in tension is really worrying because one can imagine that if, for any reason, the stress in the material in service goes over the yield strength even in narrow regions, cracks can be formed and propagate through the thickness of the tube leading to its fracture. This suggests that this material can hardly support non-uniform loadings such as those building up during temperature overshoots in service. This could possibly explain short term failures of tubes in reforming plants as repeatedly reported in the literature. Creep tests at low stress and at service temperature are necessary to better understand the mechanical behaviour of the alloy in service and the relationship with the microstructure, in particular the role of interested dendritic and eutectic networks.

REFERENCES

[1] May IL, Silveira TL, Viana CH, *International Journal of Pressure Vessels and Piping*, **66**, 1996, 233.
[2] Ray AK, Sinhaina SK, Tiwarliwari YN, Swaminathan J, Das G, Chaudhuri S, Singh R, *Engineering Failure Analysis*, **10**, 2003, 351.
[3] Shariat MH, Faraji AH, Ashrafriahy A, Alipour MM, *Corrosion Science in the 21st century*, UMIST, Manchester, **6**, 2003, paper H012.
[4] Dunlop GL, Twigg RJ, Tapplin DMR, *Scand. Journal of Metallurgy*, **7**, 1978, 152.
[5] Wen-Tai H, Honaycombe RWK, *Materials Science and Technology*, **1**, 1985, 385.
[6] Wu XQ, Jing HM, Zheng YG, Yao ZM, Ke W, Hu ZQ, *Materials Science and Engineering*, **A 293**, 2000, 252.
[7] Kirchheiner R, Woelpert P, Niobium science and technology, *TMS*, New Orleans, 2001, 1041.
[8] Jakobi D, Gommans R, *Materials and corrosion*, **54**, 2003, 881.
[9] Muralidharan G, Evans ND, Liu KC, Hemrick JG, Santella ML, Maziasz PJ, Sikka VK, Pankiw RI, *MST Conf. Proc.*, Iron Steel Technology, Warrendale, **1**, 2004, 651.
[10] Guan KS, Xu H, Wang Z, *Nuclear Engineering and Design*, **235**, 2005, 1447.
[11] Guan KS, Xu F, Wang ZW, Xu H, *Engineering Failure Analysis*, **12**, 2005, 1.
[12] Padilha AF, Rios PR, ISIJ International, **42**, 2002, 325
[13] Almeida LH, Ribeiro AF, May IL, *Materials Characterization*, **49**, 2003, 219.
[14] Chen QZ, Thomas CW, Knowles DM, *Materials Science and Engineering*, **A 374**, 2004, 398.
[15] Soares GD, Almeida LH, Silveira TL, May IL, *Materials Characterization*, **29**, 1992, 387.
[16] Wen-tai H, Honeycombe RWK, *Materials Science and Technology*, **1**, 1985, 390.
[17] Barbabela GD, Almeida LH, Silveira TL, May IL, *Materials Characterization*, **26**, 1991, 193.
[18] Haro S, Lopez D, Velasco A, Viramontes R, *Materials Chemistry and Physics*, **66**, 2000, 90.
[19] Pierkarski B, *Materials Characterization*, **47**, 2001, 181.
[20] Ribeiro AF, Almeida LH, Santos DS, Fruchart F, Bobrovnitchii GS, *Journal of Alloys and Compounds*, **356**, 2003, 693.
[21] Rodriguez J, Haro S, Velasco A, Colas R, *International Journal of Cast Metals Research*, **17**, 2004, 188.
[22] Manaurite XM Product Info, *Manoir Industries*, France.
[23] Marker^{R}/Centralloy^{R} 4852 Product Info, *Schmidt and Clemens*, Germany.